Photoelectron Spectroscopy of SiH_3^- and SiD_3^-

Mark R. Nimlos and G. Barney Ellison*

Contribution from the Department of Chemistry and Biochemistry, University of Colorado, Boulder, Colorado 80309. *Received February 20, 1986*

Abstract: We have measured the photoelectron spectra of SiH_3^- and SiD_3^- and report the following electron affinities: $EA(SiH_3) = 1.406 \pm 0.014$ eV, $EA(SiD_3) = 1.386 \pm 0.022$ eV. From an analysis of the peak splittings and intensities, we extract potential energy curves for the umbrella mode of the SiH_3^- negative ion and the SiH_3 radical. Both species are pyramidal molecules with inversion barriers of 9000 ± 2000 cm^{-1} for SiH_3^- and 1900 ± 300 cm^{-1} for SiH_3. The bond angle α(H-Si-H) for SiH_3^- is found to be 94.5° while the value for the radical, SiH_3, is 112.5°. Using the gas-phase acidity of SiH_4, we obtain the following bond dissociation energy for silane: $DH°_{298}(H_3Si-H) = 90.3 \pm 2.4$ kcal/mol.

I. Introduction

The silyl radical (SiH_3) is thought to be a pivotal species in a number of chemical systems[1,2] and may be of great importance in chemical vapor deposition processes.[3-5] Several research groups have studied[6-12] the electron spin resonance (ESR) spectroscopy of matrix-isolated SiH_3. All analyses of these ESR data conclude that the SiH_3 radical is a pyramidal molecule. Numerous ab initio calculations have been reported for this radical,[13-20] and all find the silyl radical to be a nonplanar, C_{3v}, species in excellent agreement with these ESR interpretations. Several calculations have been reported for the SiH_3^- ion as well.[21-23] An early infrared investigation[24] of silane photolysis products in a cryogenic matrix tentatively assigned several bands as belonging to the SiH_3 radical, but recent infrared studies[25] of matrix-isolated silylene (SiH_2) have raised questions about these early SiH_3 assignments. The chemistry of silanes (and SiH_3 itself) in a fast flow reactor has been summarized[26] and a recent review of the photochemistry of silanes has appeared.[27] The ionization potential of the silyl radical[15] has been measured to be $IP(SiH_3) = 8.14 \pm 0.01$ eV, while a threshold photodetachment study of SiH_3^- in an ion cyclotron resonance (ICR) spectrometer[28] finds a bound for the electron affinity: $EA(SiH_3) \leq 1.44 \pm 0.03$ eV. The solution chemistry of alkaline silyl anions such as $K^+SiH_3^-$ has been reviewed.[29] Both the NMR and infrared spectra have been reported for solutions of $K^+SiH_3^-$ in a solution of hexamethylphosphoric triamide (HMPT).[30,31]

We have measured the photoelectron spectrum of SiH_3^- and SiD_3^-. Our experiment consists of preparing a mass-analyzed ion beam and crossing it with a fixed-frequency laser. Laser photons with energy $\hbar\omega_0$ strike the negative ions and scatter electrons. We directly measure the kinetic energy (KE) of these detached electrons.

$$SiH_3^- + \hbar\omega_0 \rightarrow SiH_3 + e^-(KE) \qquad (1)$$

From an analysis of the resulting photoelectron spectrum, we can extract the binding energy of an electron to the silyl radical. By means of a Franck-Condon factor study we deduce molecular potentials for the SiH_3 radical and the SiH_3^- ion.

The experiment suggested in (1) directly measures dipole matrix elements connecting the negative ion potential surface with the radical. Consequently, it is instructive to consider the electronic structure and geometry of the SiH_3 radical and the corresponding ions, SiH_3^- and SiH_3^+. We will use a generalized valence bond (GVB) language[32,33] to do this.

One can understand[33] the structure of the silyl radical by considering silylene. Figure 1 depicts SiH_2 as a C_{2v} species with a pair of lobe orbitals strongly singlet coupled. It costs about 15 kcal/mol to uncouple this electron pair with the result that the ground state of SiH_2 is $\tilde{X}^1A_1$ about 0.75 eV below the first excited triplet state, $\tilde{a}\ ^3B_1$. The ordering of the first singlet and triplet is reversed in CH_2 where the triplet coupling is the ground state and the singlet is 0.39 eV higher in energy. Since the ground state of SiH_2 is the lobe-coupled singlet, Figure 1 (center) shows that addition of an H atom (^2S) initiates an uncoupling of the electron pair and naturally leads to a pyramidal SiH_3 radical, $\tilde{X}^2A_1$.

Ionization of SiH_2 produces the SiH_2^+ ion, Figure 1 (left). Removal of an electron from the singlet-coupled pair leads to an SiH_2^+ structure with the remaining electron in a lobe orbital sitting

(1) Gaspar, P. P. In *Reactive Intermediates*; Jones, Jr. M., Moss, R. A., Eds.; Wiley-Interscience: New York, 1981; Vol. 2, pp 335-385.
(2) Walsh, R. *Acc. Chem. Res.* **1981**, *14*, 246.
(3) White, R. T.; Espino-Rios, R. L.; Rogers, D. S.; Ring, M. A.; O'Neal, H. E. *Int. J. Chem. Kinet.* **1985**, *17*, 1029.
(4) Erwin, J.; Ring, M. A.; O'Neal, H. E. *Int. J. Chem. Kinet.* **1985**, *17*, 1067.
(5) Robertson, R.; Hils, D.; Gallagher, A. *Chem. Phys. Lett.* **1984**, *103*, 397.
(6) Jackel, G. S.; Gordy, W. *Phys. Rev.* **1968**, *176*, 443.
(7) Krusic, P. J.; and Kochi, J. K. *J. Am. Chem. Soc.* **1969**, *91*, 3938.
(8) Sharp. J. H.; and Symons, M. C. R. *J. Chem. Soc. A* **1970**, 3084.
(9) Katsu, T.; Yatsurugi, Y.; Sato, M.; and Fujita, Y. *Chem. Lett.* **1975**, 345.
(10) Raghunathan, P.; Shimokoshi, K. *Spectrochim. Acta, Part A* **1980**, *36*, 285.
(11) Nakamura, K.; Masaki, N.; Sato, S.; Shimokoshi, K. *J. Chem. Phys.* **1985**, *83*, 4504.
(12) Van Zee, R. J.; Ferrante, R. F.; Weltner, W. Jr., *J. Chem. Phys.* **1985**, *83*, 6181.
(13) Ellinger, Y.; Pauzat, F.; Barone, V.; Douady, J.; Subra, R. *J. Chem. Phys.* **1980**, *72*, 6390.
(14) Marynick, D. S. *J. Chem. Phys.* **1981**, *74*, 5186.
(15) Dyke, J. M.; Jonathan, N.; Morris, A.; Ridha, A.; Winter, M. J. *Chem. Phys.* **1983**, *81*, 481.
(16) Bunker, P. R.; Olbrich, G. *Chem. Phys. Lett.* **1984**, *109*, 41.
(17) Cartledge, F. K.; Piccione, R. V. *Organometallics* **1984**, *3*, 299.
(18) Schlegel, H. B. *J. Phys. Chem.* **1984**, *88*, 6254.
(19) Ho, P.; Coltrin, M. E.; Binkley, J. S.; Melius, C. F. *J. Phys. Chem.* **1985**, *89*, 4647.
(20) Gordon, M. S.; Truong, T. N.; Bonderson, E. K. *J. Am. Chem. Soc.* **1986**, *108*, 1421.
(21) Keil, F.; Ahlrichs, R. *Chem. Phys.* **1975**, *8*, 384.
(22) Eades, R. A.; Dixon, D. A. *J. Chem. Phys.* **1980**, *72*, 3309.
(23) Hopkinson, A. C.; Lien, M. H. *Tetrahedron* **1981**, *37*, 1105.
(24) Milligan, D. E.; Jacox, M. E. *J. Chem. Phys.* **1970**, *52*, 2594.
(25) Fredin, L.; Hauge, R. H.; Kafafi, Z. H.; Margrave, J. L. *J. Chem. Phys.* **1985**, *82*, 3542.
(26) Wörsdorfer, K.; Reimann, B.; Potzinger, P. *Z. Naturforsch., A: Phys., Phys. Chem., Kosmosphys.* **1983**, *38*, 896.
(27) Dalton, J. C. *Org. Photochem.* **1985**, *7*, 149.
(28) Reed, K. J.; Brauman, J. I. *J. Chem. Phys.* **1974**, *61*, 4830.
(29) Hengge, E. *Fortschr. Chem. Forsch.* **1974**, *51*, 1.
(30) Bürger, H.; Eujen, R. Marsmann, H. C. *Z. Naturforsch., B: Anorg. Chem., Org. Chem.* **1974**, *29*, 149.
(31) Bürger, H.; Eujen, R. *Z. Naturforsch.* B: *Anorg. Chem., Org. Chem.* **1974**, *29*, 647.
(32) Goddard III, W. A.; Dunning, T. H.; Hunt, W. J.; Hay, P. J. *Acc. Chem. Res.* **1973**, *6*, 368.
(33) Goddard III, W. A.; Harding, L. B. *Annu. Rev. Phys. Chem.* **1978**, *29*, 363.

0002-7863/86/1508-6522$01.50/0

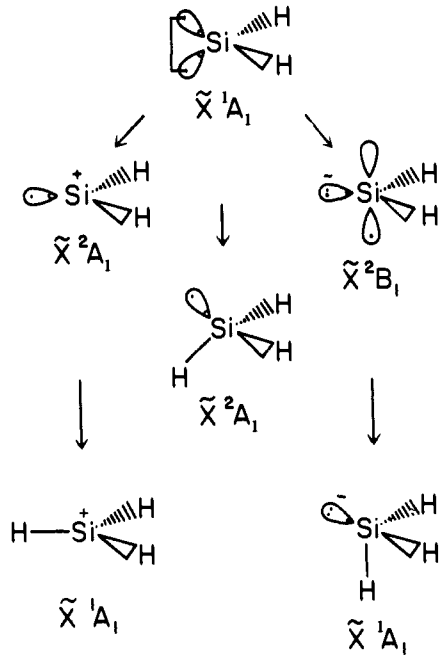

Figure 1. GVB diagrams showing the formation of SiH_3^+, SiH_3, and SiH_3^- from silylene and atomic hydrogen.

in the molecular plane; the positive, electron hole is an "empty" π-type orbital at right angles to the two Si–H bonds and the singly filled lobe. Addition of an H atom to SiH_2^+ directly leads to a flat, D_{3h} ion, SiH_3^+. This cation is designated $\tilde{X}^1A_1$ (Figure 1, left).

The SiH_3^- negative ion can be constructed from the SiH_2^- anion. Addition (Figure 1, right) of an extra electron to SiH_2 uncouples the singlet pair and leads to a doubly occupied, in-plane orbital and an out-of-plane, singly occupied π-type orbital. SiH_3^- results from addition of a H atom to SiH_2^-. The hydrogen atom can only combine with SiH_2^- in one way. The new Si–H bond must be formed at right angles to the existing pair of Si–H bonds; formation of a "planar" Si–H bond is defeated by the presence of the doubly occupied orbital. These notions suggest that the SiH_3^- ion is strongly pyramidal and is likely to have tight H–Si–H bond angles, say $\alpha(SiH_3^-) \simeq 100°$. In contrast, the silyl radical should have bond angles near to the tetrahedral value, $\alpha(SiH_3) \simeq 109°$, while the cation must be perfectly flat, $\alpha(SiH_3^+) = 120°$.

This simple picture suggests that detachment of the SiH_3^- ion to produce electrons and the SiH_3 radical (eq 1) will be accompanied by a significant geometry change. There are only four vibrational modes in a symmetric AH_3 molecule: ω_1, the symmetric stretch; ω_2, the symmetric bend; ω_3, the asymmetric stretch; and ω_4, the asymmetric bend. Use of the Condon approximation implies that only the symmetric modes [A_1: ω_1 and ω_2] can be excited upon detachment while the asymmetric vibrations [E: ω_3 and ω_4] are forbidden degrees of freedom. One expects to observe a strong progression in the symmetric bending mode of SiH_3 which is calculated to be about 800 cm^{-1}. We can estimate a frequency for the SiH_3^- ion by considering the isoelectronic species, phosphine.[34] The umbrella mode, ω_2, occurs at 992 cm^{-1} in PH_3 and falls to 730 cm^{-1} in PD_3. The umbrella frequency of SiH_3^- will be higher than that of the silyl radical and lower than the values for phosphine; we expect the umbrella mode for SiH_3^-, ω_2, to be in the range 850 and 950 cm^{-1}. Infrared and Raman studies[31] of $K^+SiH_3^-$ in HMPT solution have reported assignments of ω_2 = 865 (?) cm^{-1} for SiH_3^- and ω_2 = 635 cm^{-1} for SiD_3^-.

II. Experimental Section

The experimental hardware which we use to carry out (1) has been described in some detail elsewhere.[35,36] Ions are prepared in a high-pressure (approximately 0.1 torr) dc, electrical discharge from a 4:1 mixture of silane and ammonia, mass-selected with a Wien filter, and delivered to a high-vacuum chamber for detachment. Figure 2 shows the negative ion mass spectrum that is extracted from this source. Peaks assigned as NH_2^-, Si^-, and SiH^- are identified by their photoelectron spectra which agree with established values.[37,38] The intense feature at m/z 31 is attributed to SiH_3^-; as we shall see there is a small component of SiH_2^- buried under this peak. In most experiments we work with mass-selected ion beam currents of roughly 0.5 nA.

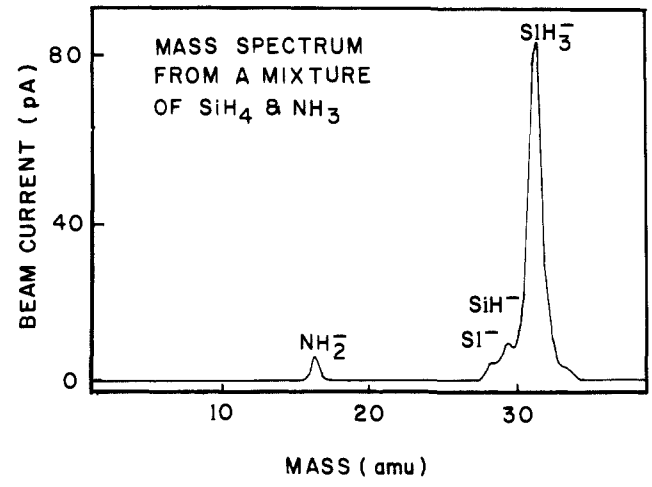

Figure 2. Negative ion mass spectrum resulting in a discharge of silane and ammonia.

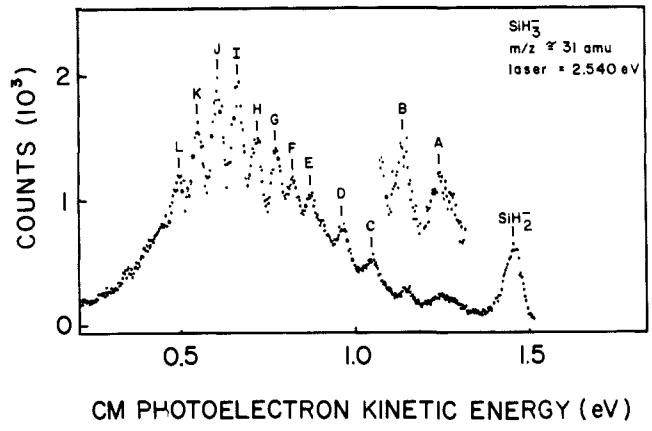

Figure 3. Photoelectron spectrum of SiH_3^-; the data points are separated by roughly 2.8 MeV.

The ion beam is crossed with the output of an Ar II laser operating CW on a single line (λ_0 = 488 nm or $\hbar\omega_0$ = 2.540 eV); the laser maintains about 75 W of intracavity power. Detached electrons are collected and analyzed by a pair of hemispherical analyzers; these electrostatic analyzers operate with a resolution of roughly 20 MeV (fwhm) as measured with a beam of O^- ions. The photoelectron spectrum must be calibrated with a reference ion and transformed to the center of mass (CM) frame. We use OH^- as a calibration ion[37] with $EA_{cal}(OH)$ = 1.829 ± 0.009 eV and M_{cal} = 17 amu. We use the following expression to calculate the KE in the CM frame.

$$KE = KE_{cal} + \gamma(V_{cal} - V) + mW[M^{-1} - M_{cal}^{-1}] \qquad (2)$$

In (2) KE is the CM energy (eV) of an electron detached from an ion of mass M (amu) which is passed by the energy analyzer when the slit voltage is V. The CM kinetic energy of the calibration ion is KE_{cal} ($\hbar\omega_0 - EA_{cal}$). The slit voltage at the center of the calibration ion's peak is V_{cal} while γ is a dimensionless scale compression factor (typically 1.007 ± 0.010) measured from the Cr^- photoelectron spectrum.[39] The ion

(34) Shimanouchi, T. "Tables of Molecular Vibrational Frequencies"; *Natl. Stand. Ref. Data Ser.* **1972**, Consolidated Vol. 1, NBS 39.
(35) Ellis, H. B., Jr.; Ellison, G. B. *J. Chem. Phys.* **1983**, *78*, 6541.
(36) Ellis, H. B., Jr. Ph.D. Thesis, University of Colorado, 1983.
(37) Celotta, R. J.; Bennett, R. A.; Hall, J. L. *J. Chem. Phys.* **1974**, *60*, 1740.
(38) Kasdan, A.; Herbst, E.; Lineberger, W. C. *J. Chem. Phys.* **1975**, *62*, 541.
(39) Feigerle, C. S.; Corederman, R. R.; Bobashev, S. V.; Lineberger, W. C. *J. Chem. Phys.* **1981**, *74*, 1580.

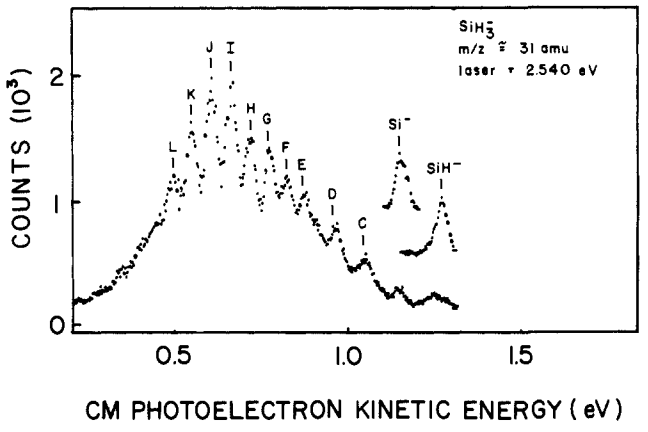

Figure 4. The mass spectrum from Figure 3 with the peak positions of Si^- and SiH^- plotted as insets.

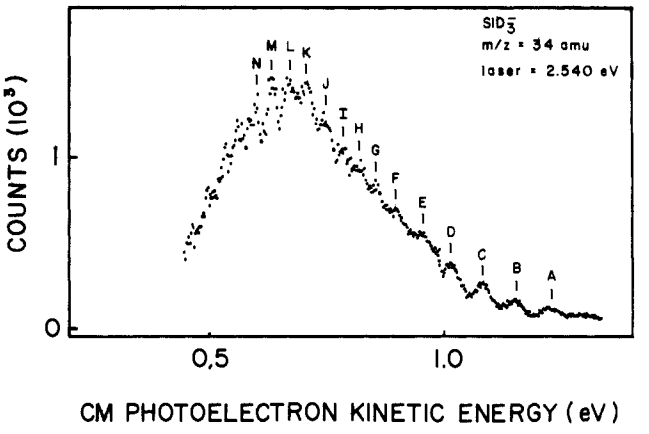

Figure 5. Photoelectron spectrum of SiD_3^-; the data points are separated by roughly 2.8 MeV.

Table I. Photoelectron Spectrum of SiH_3^- (Laser λ_0 = 488 nm)

peak	CM KE (eV)	peak intervals (cm^{-1})	splitting from origin (cm^{-1})	assignment
A	1.249 ± 0.017		880	2_1^0
		880		
B	1.140 ± 0.012			(0,0)
		750		
C	1.047 ± 0.016		750	$2_6^1\pm$
		670		
D	0.964 ± 0.011		1420	$2_0^2\pm$
		740		
E	0.871 ± 0.011		2170	2_0^3-
		410		
F	0.822 ± 0.011		2560	2_0^4+
		400		
G	0.773 ± 0.008		2960	2_0^4-
		460		
H	0.717 ± 0.013		3410	2_0^5+
		440		
I	0.662 ± 0.013		3860	2_0^5-
		440		
J	0.608 ± 0.013		4290	2_0^6+
		480		
K	0.548 ± 0.009		4770	2_0^6-
		440		
L	0.494 ± 0.016		5210	2_0^7+

Table II. Photoelectron Spectrum of SiD_3^- (Laser λ_0 = 488 nm)

peak	CM KE (eV)	peak intervals (cm^{-1})	splitting from origin (cm^{-1})	assignment
A	1.225 ± 0.025		580	2_1^0
		580		
B	1.155 ± 0.021			(0,0)
		560		
C	1.085 ± 0.020		560	$2_0^1\pm$
		570		
D	1.015 ± 0.021		1130	$2_0^2\pm$
		510		
E	0.955 ± 0.024		1610	$2_0^3\pm$
		440		
F	0.900 ± 0.024		2060	2_0^4-
		310		
G	0.861 ± 0.022		2370	2_0^5+
		310		
H	0.823 ± 0.024		2680	2_0^5-
		280		
I	0.788 ± 0.025		2960	2_0^6+
		310		
J	0.750 ± 0.024		3270	2_0^6-
		320		
K	0.710 ± 0.024		3590	2_0^7+
		310		
L	0.672 ± 0.024		3900	2_0^7-
		260		
M	0.637 ± 0.022		4180	2_0^8+
		350		
N	0.594 ± 0.024		4520	2_0^8-

beam kinetic energy is W (eV) while m is the mass of an electron (amu).

Silane was purchased from Petrarch and used without further purification. Our deuterated silane came from two sources. One batch was acquired from Cambridge Isotope gas and another was synthesized. Silane-d_4 was prepared by an established procedure[40] in which $SiCl_4$ was dissolved in a Et_2O solution and slowly added to a refluxing solution of Et_2O and $LiAlD_4$. The product was passed through a -95 °C trap and condensed in a vessel cooled by liquid nitrogen. The product SiD_4 was purified by trap-to-trap distillation through five -130 °C traps and collected in a final container at -196 °C.

III. Results

Figure 3 shows the photoelectron spectrum that results from detachment of the m/z 31 ion beam. There is intense feature at a KE of 1.45 eV and an extensive progression covering the range of KE from 0.5 to 1.3 eV. The peak at 1.45 eV is definitely due to detachment of SiH_2^-; the EA of this feature is 1.087 ± 0.018 eV in agreement with the established value.[38] By varying the pressure in our discharge ion source, we can drastically alter the appearance of the SiH_2^- peak; under certain conditions it is the strongest band in the entire spectrum while with others this feature can be obliterated. The only peaks that we will consider as belonging to SiH_3^- are those labeled A–L.

The weak features labeled A and B seem to be unusually broad and the inset in Figure 3 has been enhanced by a factor of 10. Part of the difficulty with these peaks was revealed when we separately detached beams of Si^- and SiH^- and found that signals from these ions fall right in the region of A and B. Figure 4 emphasizes this misfortune; we have replotted a portion of Figure 3 and show features from Si^- and SiH^- plotted as insets. The spectroscopy of Si^- and SiH^- is well known[38] so there is no question as to the identity or peak location of these ions. Inspection of Figure 4 suggests that our peaks A and B may be blended with weak signals belonging to these contaminating ions, Si^- and SiH^-. Our apparent difficulties with the "purity" of our m/z 31 ion beam stem from the fact that the silane discharges in our ion source are unstable. The current of SiH_3^- is so much stronger than any of the other silicon ions that it is difficult to exclude Si^-, SiH^-, and SiH_2^- altogether. The presence of silicon isotopes [^{29}Si (4.7%)

(40) Norman, A. D.; Webster, J. R.; Jolly, W. L. *Inorg. Synth.* **1968**, *11*, 170.

(41) Bartmess, J. E.; Scott, J. A.; McIver, R. T. Jr., *J. Am. Chem. Soc.* **1979**, *101*, 6046. Kass, S. R.; Filly, J.; Van Doren, J.; Nimlos, M. R.; Bierbaum, V. M., unpublished results.

(42) Drs. Jasinski, J. J. (IBM Yorktown Heights) and Houle, F. A. (IBM, San Jose) have separately lectured us about the importance of these thermodynamic values.

(43) The literature describing this potential is huge. See: Coon, J. B.; Naugle, N. W.; McKenzie, R. D. *J. Mol. Spectrosc.* **1966**, *20*, 107.

(44) Bunker, P. R.; Kraemer, W. P.; Spirko, V. *Can. J. Phys.* **1984**, *62*, 1801.

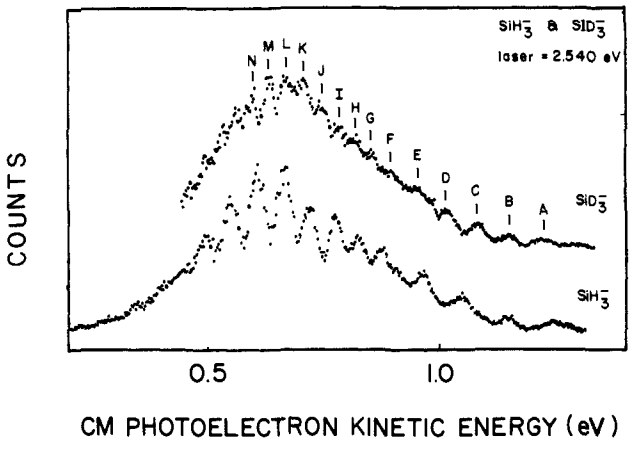

Figure 6. Composite figure which contains data for SiH_3^- (from Figure 3) and for SiD_3^- (from Figure 5) offset from each other to illuminate the peak shifts.

and ^{30}Si (3.1%)] also contributes to our difficulties. When we examine SiD_3^- at m/z 34, we experience none of these problems.

The A–L peak positions (in eV) are collected together in Table I as well as the peak intervals (in cm^{-1}); the two right-hand columns will be discussed later. On account of the uncertainties due to possible Si^- and SiH^- contamination, we cannot use many of our techniques to search for SiH_3^- hot bands. Hot bands are features which result from detachment of vibrationally excited negative ions and are generally assigned by varying the ion source conditions or changing the ion precursor. Such a strategy will not be convincing in the present case since tiny variations in the contaminating ions (Si^- and SiH^-) would manifest themselves in fluctuations of peaks A and B. Fortunately in this case SiD_3^- allows us to identify the origin and assign the single hot band. The photoelectron spectrum of SiD_3^- is shown in Figure 5 and tabulated in Table II. The SiD_3^- at m/z 34 is free from contamination by other negative ions. Figure 6 plots the data from Figure 3 (SiH_3^-) and Figure 5 (SiD_3^-) in order to illuminate relative peak shifts.

IV. Discussion

Figure 6 allows us to identify the (0,0) band of the SiH_3^- photoelectron spectrum. The B peak does not shift upon deuteration while all other features in the spectrum do. The features (C, D, ..., N) in SiD_3^- all collapse to higher KE toward the B peak, but the A peak shifts in the other direction. It is implied that (a) peak B is the origin of the photoelectron spectrum while A results from detachment of a vibrationally excited SiH_3^- ion, (b) there is a significant geometry difference between SiH_3^- and SiH_3, and (c) a low-frequency mode is active in the detached SiH_3 radical. The identification of B as the (0,0) band immediately produces values for the uncorrected electron affinities: EA(SiH_3) = 1.400 ± 0.012 eV and EA(SiD_3) = 1.385 ± 0.021 eV. A correction must be made to the EA to reflect the fact that our negative ions are spread over a variety of rotational and vibrational states. These small corrections will be estimated at the end of the paper.

We now turn to an analysis of the spectra shown in Figure 4 and 5. From the GVB ideas sketched in Figure 1 we expect the photoelectron spectrum of SiH_3 to feature a progression in the silyl radical bending mode. This is certainly the case; reference to Tables I and II shows quite clearly that the active mode in SiH_3 has a low frequency. Since we only have the symmetric stretch (ω_1) and the umbrella mode (ω_2) to choose from, the identiciation of the progression in Figure 4 and 5 as ω_2 in unambiguous. Notice (Table I) that the vibrational intervals are about 700 cm^{-1} up to the E peak while the splittings above the G peak are roughly 450 cm^{-1}. Since SiH_3 is a nonplanar molecule, suppose that the barrier to inversion is approximately 1000–2500 cm^{-1}. If the inversion splitting is small ($\simeq$50 cm^{-1} or less), one might see a simple progression at a high frequency below the top of the barrier; the apparent frequency will drop by about half above the barrier as the vibrational levels mix and split.

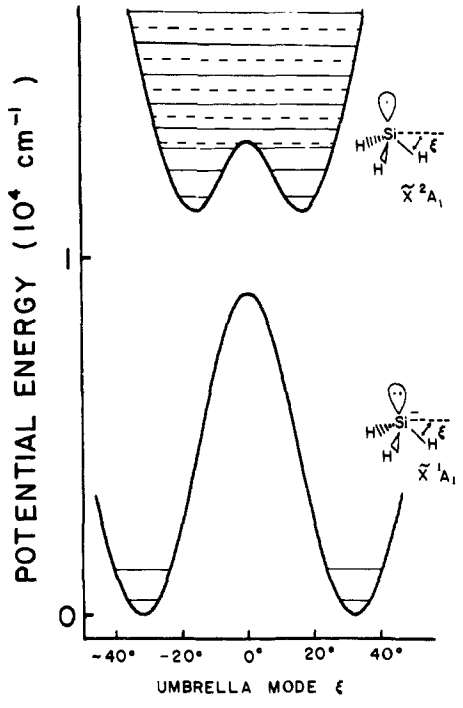

Figure 7. Curves used to model the symmetric bending potential (ω_2) of SiH_3^- and SiH_3. The vibrational energy levels are calculated by variationally solving a model Hamiltonian (Table III). Each quantum level is doubly degenerate below the barrier; above the barrier the inversion splitting becomes large enough to observe, and a dashed line (---) depicts the second member of an inversion doublet.

We have used a simple oscillator to model both the silyl radical and the silyl anion. One can represent[45] the umbrella mode (ω_2) in a pyramidal species by a linear oscillator perturbed by a Gaussian barrier.

$$V(X_2) = \tfrac{1}{2}k_2X^2 + D\exp(-\beta X_2^2) \qquad (3)$$

We have used (3) as the potential in a vibrational Schrödinger equation and approximated the mass of the oscillator with the simple G-matrix element, $g_2 = [3M_HM_{Si}/(3M_H + M_{Si})]^{-1}$. The independent variable, X_2, is most simply written as $r_0\xi$ where r_0 is the equilibrium Si–H bond length and ξ is the out-of-plane bending angle. Throughout the Franck-Condon analysis we have constrained r_0 at the calculated[16] value of 1.481 Å. The final Schrödinger equation is solved by a variationally correct manner in a basis of B-splines. We have chosen parameters, k_2, D, and β, to fit the SiH_3^- data in Figure 4. Table III collects these formulas together and lists the final parameters for both the silyl radical and the silyl anion. Figures 7 and 8 display the final potentials and energy levels calculated for SiH_3^- and SiD_3^-. These potentials suggest that the SiH_3 is bent out of the plane by 16.0 ± 2.0° corresponding to an H–Si–H angle of $\alpha(SiH_3)$ = 112.5 ± 2.0°; the inversion barrier in SiH_3 is calculated to be 1900 ± 300 cm^{-1}. In contrast the silyl anion is bent 32.0 ± 2.0° out of the plane with $\alpha(SiH_3^-)$ = 94.5 ± 2.0°; the inversion barrier for the SiH_3^- ion is conjectured to be 9000 ± 2000 cm^{-1}. Since we can only assign a single hot band (peak A) we cannot determine the barrier for the anion as well as that for SiH_3.

One can get a feeling for the accuracy of our fit by looking at Figure 9. The points are the experimental data for SiH_3^- while the solid line is the computed spectrum that results from the potentials displayed in Figure 7. The sticks in Figure 9 are the individual transitions which are then folded with a Gaussian line shape with an empirically determined line width of 45 meV and weighted with a Boltzmann factor. This Boltzmann factor uses 600 ± 400 K as the effective vibrational temperture for the

(45) Radziszewski, J. G.; Michl, J.; Ellison, G. B. unpublished results.

Table III. Vibrational Schrödinger Equation: SiH_3 Umbrella Mode (ω_2)

A. Formulas[45]

$$V(X_2) = {}^1/_2 k_2 X_2^2 + D\exp(-\beta X_2^2)$$

$$X_2 = \frac{r(\mathrm{SiH})\xi\pi}{180} \text{ and } \rho = \ln(2D\beta/k_2)$$

$$\alpha(\mathrm{H\text{-}Si\text{-}H}) = 2\sin^{-1}[(3/4)^{1/2}\cos\xi]$$
$$\text{barrier} = b = D(e^{\rho} - \rho - 1)e^{-\rho}$$

$$\xi_{min}^2 = \frac{\rho}{\beta}\left[\frac{180}{\pi r(\mathrm{SiH})}\right]^2$$

B. Fitting Parameters

radical	anion
r_0(SiH) constrained at 1.481 Å during fits of both radical and ion	
$k_2' = 17072\ \mathrm{cm^{-1}\ Å^{-2}}$	$k_2'' = 16275\ \mathrm{cm^{-1}\ Å^{-2}}$
(0.39913 mdyn $\mathrm{Å^{-2}}$)	(0.32330 mdyn $\mathrm{Å^{-1}}$)
$D' = 4894\ \mathrm{cm^{-1}}$	$D'' = 17859\ \mathrm{cm^{-1}}$
$\beta'' = 7.87654\ \mathrm{Å^{-2}}$	$\beta'' = 2.48193\ \mathrm{Å^{-2}}$

C. Final Results

$\xi_{min}' = 16.0 \pm 2.0°$	$\xi_{min}'' = 32.0 \pm 2.0°$
$\alpha(\mathrm{H\text{-}Si\text{-}H})' = 112.5 \pm 2.0°$	$\alpha(\mathrm{H\text{-}Si\text{-}H})'' = 94.5 \pm 2.0°$
$b' = 1900 \pm 300\ \mathrm{cm^{-1}}$	$b'' = 9000 \pm 2000\ \mathrm{cm^{-1}}$

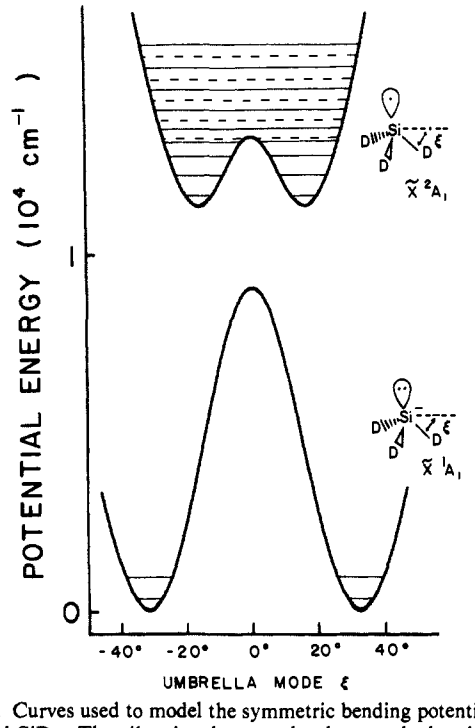

Figure 8. Curves used to model the symmetric bending potential (ω_2) of SiD_3^- and SiD_3. The vibrational energy levels are calculated by variationally solving a model Hamiltonian (Table III). Each quantum level is doubly degenerate below the barrier; above the barrier the inversion splitting becomes large enough to observe and a dashed line (---) depicts the second member of an inversion doublet.

negative ions. This is to be compared with the vibrational temperature found earlier[35] for O_2^- of 450 ± 150 K.

There are some difficulties with the relative intensities of several of the peaks at both ends of the spectrum, but the fit to the experimental data is plausible. An excellent test for our model is to fit the data for SiD_3^-. Within the Born–Oppenheimer model the same potentials that we have used for the d_0 ion must also be employed for the d_3 isomer. When the potentials from Table III and Figure 8 are used to calculate a photoelectron spectrum for SiD_3^-, the result is Figure 10. Again we directly compare the experimental data (points) with the modeled spectrum (solid line). While the fit in Figure 10 has intensity difficulties in some places, most of the line positions are accurately predicted. Figures

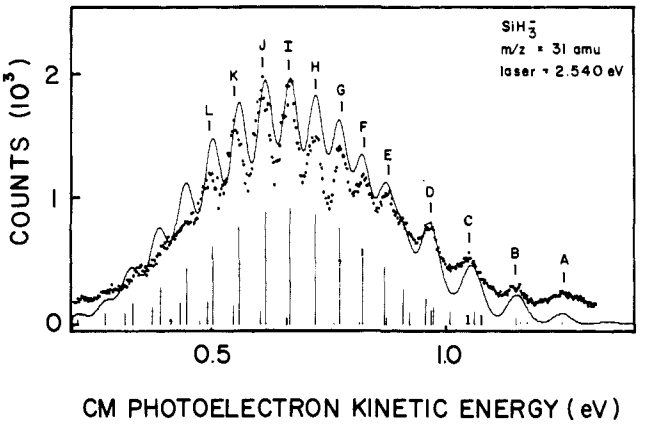

Figure 9. A high signal-to-noise photoelectron spectrum of SiH_3^-. The points are the experimental spectrum from Figure 3 while the solid line is a calculated spectrum for comparison. The modeled spectrum results from a Franck-Condon calculation using the potential curves in Figure 7.

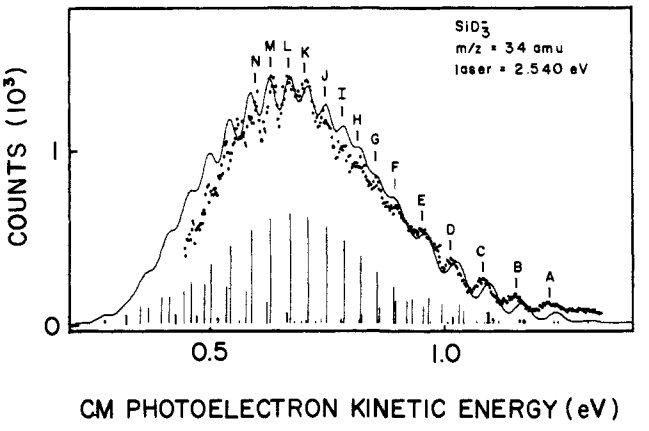

Figure 10. A high signal-to-noise photoelectron spectrum of SiD_3^-. The points are the experimental spectrum from Figure 5 while the solid line is a calculated spectrum for comparison. The modeled spectrum results from a Franck-Condon calculation using the potential curves in Figure 8.

Table IV. Calculated Silyl Radial and Anion Properties[a]

ω_1(sym str)	ω_2(umbrella)	ω_3(asym str)	ω_4(asym bend)	barrier	α(H-Si-H) (deg)	ref
			SiH_3			
2140	847				111.3	13
	702				112.6	14
2300	820				110.6	15
2424	778	2106	976	1951	111.2	16
				1768	111.7	17
2275	784	2292	989		108.0	18
2364	875	2383	1015			19
2344	857	2365	1010			20
			SiH_3^-			
				9164	97.6	21
				9101	97.0	22
				11997	95.3	23

[a] Ab initio calculations of the inversion barrier, vibrational frequencies, and bond angles; all energies are in $\mathrm{cm^{-1}}$ and the angles in deg.

9 and 10 suggest that our naive model in Table III is qualitatively correct.

Our experimental parameters are in reasonable agreement with the computational values that are collected together in Table IV. The most precise SiH_3 calculations are those of Bunker and Olbrich[16] who have used a multireference determinant CI technique to generate 64 points on the ground electronic energy surface, $\tilde{X}^2A_1$; this surface leads to an equilibrium geometry of $r_0 = 1.480$ Å and $\alpha(SiH_3) = 111.2°$. Use of a nonrigid invertor

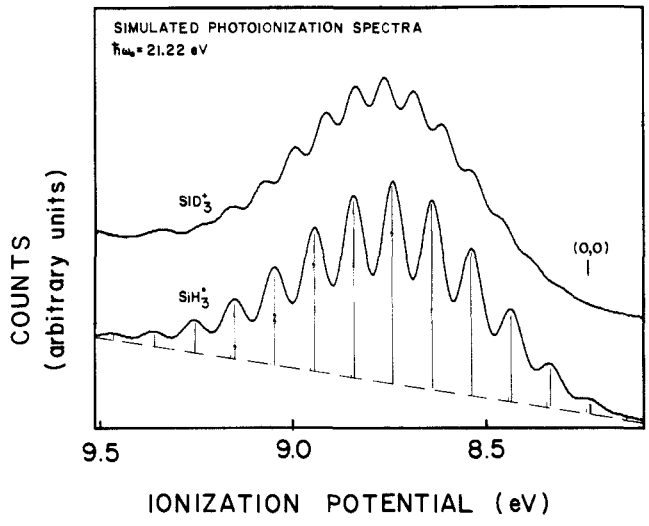

Figure 11. Calculated photoionization spectra for SiH_3 and SiD_3^+; we have used the potential from Table III for the silyl radical and treated the cation as a simple harmonic oscillator with an umbrella frequency[15] of 820 cm^{-1} for the d_0 ion. The SiH_3^+ prediction can be compared with the experimental spectrum shown in Figure 1 of ref 15.

Hamiltonian with their ab initio potential completely determines the vibrational levels for SiH_3 (see Table IV). For SiD_3 the theoretical vibrational frequencies fall to ω_1 = 1698 cm^{-1}, ω_2 = 588 cm^{-1}, ω_3 = 1,568 cm^{-1}, and ω_4 = 701 cm^{-1}. Our vibrational fundamentals (750 and 560 cm^{-1}; Tables I and II) agree quite well the nonrigid invertor predictions for ω_2. Our hot bands furnish values for the umbrella mode of SiH_3^- (880 cm^{-1}) and SiD_3^- (580 cm^{-1}); the closeness of the infrared values reported from a solution study[31] (865 and 635 cm^{-1}) is impressive.

We can use the results of the photoionization of SiH_3 as an additional qualitative test of our silyl radical potential (Table III). It was concluded[15] that SiH_3^+ is a planar, D_{3h}, cation with a harmonic frequency, ω_2 = 820 cm^{-1}, and a Si–H bond length of 1.45 Å. This is entirely in accord with one's expectations set forth in Figure 1. We have used our SiH_3 potential (Table III) and SiH_3^+ potential of Dyke et al. to simulate the photoionization spectra for SiH_3 and SiD_3. Using these potentials, we have constructed the vibrational wavefunctions for both the silyl radical and the silyl cation. We then numerically integrate the overlap of the vibrational wavefunctions to generate the Franck-Condon factors for the process:

$$SiH_3 + \hbar\omega_0 \rightarrow SiH_3^+ + e^-(KE) \qquad (4)$$

We have used a vibrational temperature of 300 K which was proposed by Dyke et al. In the photoionization experiments, a helium resonance lamp is employed so that $\hbar\omega_0$ = 21.22 eV in eq 4. The results of our SiH_3 photoionization modeling are displayed in Figure 11. In modeling the photoionization experiment it is necessary[15] to include a sloping background to simulate the rising experimental baseline which is alleged to arise from the weak He Iγ and He Iδ ionizations of SiH_4.

We have simply identified the most intense feature in Figure 11 as the vertical IP (Dyke et al.'s peak *G*) and assigned it their binding energy of 8.74 ± 0.01 eV. Having fixed peak G in Figure 11 at 8.74 eV, we find the (0,0) band in our simulated spectrum to fall at 8.23 eV. This is one quantum higher than the Southampton results. A comparison of Figure 11 and Figure 1 in ref 15 reveals that our simulation (Figure 11) fits the experimental photoionization data at least as well as Dyke et al.'s calculation. We have gone ahead to predict the photoionization spectrum of SiD_3, and our results are depicted at the top of Figure 11. Use of the SiH_3^+ potential in our vibrational Schrödinger equation leads to a predicted frequency of $\omega_2(SiD_3^+)$ = 605 cm^{-1} and an estimated vertical IP for SiD_3 of 8.76 ev. Our conjectures about the photoionization spectrum of SiD_3 are in agreement with Dyke et al.'s experimental findings; they report that the ionization spectrum of SiD_3 is a broad band centered at 8.74 ± 0.02 eV.

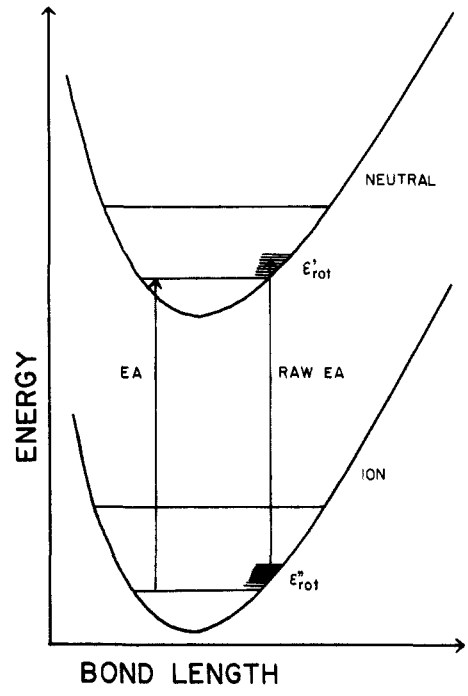

Figure 12. A set of potential energy curves to outline the notation used to describe the rotational correction and the sequence band adjustment to the electron affinity.

The Franck-Condon profile for the photoionization of SiH_3 is quite sensitive to degree of nonplanarity of the silyl radical. We wish to suggest that the (0,0) of the ionization profile might be revised upward in the future. Based on our silyl bond angle $\alpha(SiH_3)$ of 112.5 ± 2.0°, we suggest that the experimental photoionization spectrum of ref 15 might be interpreted to assign $IP(SiH_3)$ one vibrational quantum higher at 8.23 eV rather than 8.14 eV. These modifications differ very slightly from those suggested by the photoionization study [$IP(SiH_3)$ = 8.14 ± 0.01 eV and $\alpha(SiH_3)$ = 110.6°]. Indeed, the coincidence of our parameters which are independently derived from a study of the negative ion, SiH_3^-, with those emanating from a study of the positive ion, SiH_3^+, is quite impressive.

It might be useful to estimate the vibrational frequencies of SiH_3 and SiD_3 in a cryogenic matrix. The calculations of Bunker and Olbrich[16] seem to be a reasonable guide for the gas-phase frequencies of the silyl radical. We estimate that their frequencies are accurate to ±5% or better by comparing the calculated[44] values with those measured experimentally for ammonia.[34] A conjecture of the gas-to-crystal shift for SiH_3 can be made by using NH_3 in a similar fashion. Let us match the gas-phase[34] frequencies (in cm^{-1}) with those for NH_3 in an argon matrix[45] at 14 K (the matrix values are in parentheses): ω_1 = 3336.02 (3345), ω_2 = 932.42 (974), ω_3 = 3443.63 (3447), and ω_4 = 1626.30 (1638). By taking ratios of these frequencies, we can correct the nonrigid invertor values and estimate vibrational frequencies of SiH_3 and SiD_3 (shown in parentheses) in an argon matrix: ω_1 = 2431 (1703), ω_2 = 813 (614), ω_3 = 2108 (1570), and ω_4 = 983 (706). Efforts are now underway[45] to prepare the silyl radical and record its infrared spectrum in an argon matrix, but little progress has been made beyond earlier efforts.[24]

V. Thermochemistry

The EA properly corresponds to the $|SiH_3(v' = 0, J'K' = 0)\rangle \leftarrow |SiH_3^-(v'' = 0, J''K'' = 0)\rangle$ transition. In order to obtain the adiabatic EA, we must make a rotational correction and a sequence band adjustment to the uncorrected, or raw EA.

Let us consider the rotational correction first. This problem is outlined in Figure 12 which shows detachment from a negative ion to a final neutral. The ions populate a variety of rotational levels, and this ion distribution has a mean rotational energy, ϵ_{rot}''. The raw EA we measure is a transition from a set of levels with ϵ_{rot}'' to a set of final neutral states with an average rotational

Table V. Experimental Molecular Properties[a]

	cation		radical		anion	
	SiH_3^+	SiD_3^+	SiH_3	SiD_3	SiH_3^-	SiD_3^-
ω_2(umbrella), cm^{-1}	820	605	750	560	880	580
inversion barrier, cm^{-1}	0		1900 ± 300		9000 ± 2000	
α(H-Si-H), deg	0		112.5 ± 2.0		94.5 ± 2.0	
B, cm^{-1}	5.32	2.67	4.79	2.44	4.15	2.17
C, cm^{-1}	2.66	1.34	2.71	1.39	3.54	1.78
$\Delta H_f°_{298}$, ckal/mol	234.1 ± 2.4		46.4 ± 2.4		14.0 ± 2.4	

[a] $EA(SiH_3)$ = 1.406 ± 0.014 eV, $EA(SiD_3)$ = 1.386 ± 0.022 eV, $IP(SiH_3)$ = 8.14 ± 0.01 eV.

energy, ϵ_{rot}'. It is apparent that the raw EA and the proper EA are simply related.

$$\text{raw EA} = \text{EA} - \epsilon_{rot}'' + \epsilon_{rot}' \quad (5)$$

If we define a rotational correction like $\Delta_{rot} = [\epsilon_{rot}' - \epsilon_{rot}'']$, we can extract the proper EA from the uncorrected EA: EA = raw EA − Δ_{rot}.

We make the rotational correction[46] by treating both the ion and radical as simple oblate tops and by estimating the rotational constants (B and C) with the help of the molecular geometries in Table III. Our working expression for the rotational correction is:

$$\Delta_{rot} = k_B T_{rot}[(B'/B'') + (C'/2C'') - (3/2)] \quad (6)$$

The Boltzmann constant is written as k_B and we use a rotational temperature, T_{rot}, of 600 K. The final resulting corrections turn out to be quite small; $\Delta_{rot}(SiH_3)$ = 0.0019 ± 0.0045 eV and $\Delta_{rot}(SiD_3)$ = 0.0008 ± 0.0030 eV.

There is an additional correction which must be estimated. This results from sequence bands[48] and can be understood in the following manner. Reference to the vibrational levels in Figure 12 indicates that (1,1) = (0,0) − [$\omega'' - \omega'$]; consequently, if we detach a highly vibrationally excited ion we will find transitions shifted away from the proper (0,0) or EA by an amount proportional to the difference of the vibrational frequencies. By the blending together of the origin, (0,0), with the sequence band, (1,1), the centroid of the first peak will be pulled away from the proper EA. The amount of the shift cannot exceed [$\omega'' - \omega'$] and in our present case (Table I) this value is [880 cm^{-1} − 750 cm^{-1}]. Thus EA = raw EA + Δ_{seq}, where Δ_{seq} is some fraction of 130 cm^{-1}. Commonly we will conjecture that $\Delta_{seq} \simeq \eta(\Delta\omega)$. The fraction, η, will depend upon the relative ion populations of v'' = 1 and v'' = 0 in the beam and upon the ratio of the Franck-Condon factors, FCF(1,1)/FCF(0,0). We estimate that η is about 0.5 so that $\Delta_{seq}(SiH_3^-)$ = 0.008 ± 0.007 eV and $\Delta_{seq}(SiD_3^-)$ = 0.002 ± 0.007 eV. Thus we finally arrive at the corrected values for the electron affinities: $EA(SiH_3)$ = 1.406 ± 0.014 eV and $EA(SiD_3)$ = 1.386 ± 0.022 eV.

Recent experiments[49] report a SiH_3^- photodetachment threshold at λ_0 = 842 ± 2 nm corresponding to an $EA(SiH_3)$ = 1.473 ± 0.003 eV. This value is incompatible with our interpretation of the photoelectron spectra (Figures 4–6). An $EA(SiH_3^-)$ of 1.473 eV could be accommodated by our data if we assigned peak C in Figures 4 and 5 as the origin of the spectrum. This suggests that our features A and B are hot bands. In the light of the SiD_3^- spectrum (Figure 5), we think that this is unlikely. Upon deuteration the peak positions of the silyl radical will shift. Because the umbrella mode is not a simple, linear oscillator, we cannot make a reasonable back of the envelope calculation. The usual way to proceed is to consider the umbrella mode of SiH_3 as a harmonic oscillator and use a simple expression for the energy levels such as:

$$G_v(\omega_2) = \omega_2(v + \tfrac{1}{2}) - x_{22}(v + \tfrac{1}{2})^2 \quad (7)$$

Since the anharmonicity constant, x_{22}, is always much less than the frequency, eq 7 is roughly a monotonic function of v_2. One normally uses a G-matrix element to make a conjecture of the isotope shift between SiH_3 and SiD_3 frequencies, ω_2:

$$\omega_2(SiD_3) \simeq \{[3M_HM_{Si}/(3M_H + M_{Si})]/[3M_DM_{Si}/(3M_D + M_{Si})]\}^{1/2}\omega_2(SiH_3) \quad (8)$$

With 750 cm^{-1} assigned to ω_2, use of (8) suggests that the umbrella frequency of SiD_3 should be roughly 0.74 × 750 or 556 cm^{-1}.

Application of (7) to the silyl radical and ion leads to an isotopic shift of the origin of a few MeV. Transitions to the higher SiH_3 vibrational states are shifted by larger and larger amounts. Because peak B suffers the smallest isotopic shift, we are inclined to assign it to the (0,0) band. This assignment would imply photodetachment thresholds of $\lambda_0(SiH_3)$ = 882 ± 9 nm and $\lambda_0(SiD_3)$ = 895 ± 14 nm. Since the active electron in SiH_3^- is detached from an a_1 orbital (which transforms like an "s orbital"), the outgoing electron is likely to be predominantly a "p-wave". The detachment cross section (σ) at threshold should vary with energy as $\sigma(E) \simeq E^{3/2}$. This is a slowly rising threshold and may be difficult to identify at the long wavelengths (880–900 nm) that we predict. The reduced (0,0) Franck-Condon factor makes this a difficult measurement.

The gas-phase acidity of silane has been measured[41] earlier in an ICR spectrometer to be 371.5 ± 2.4 kcal/mol; this has been confirmed in separate experiments on a flowing afterglow device. The gas-phase acidity is defined to be the enthalpy of the heterolytic bond dissociation.

$$SiH_3\text{–}H \rightarrow SiH_3^- + H^+ \quad (9)$$

We can use the $EA(SiH_3)$ and the acidity to calculate the bond strength of silane.

$$DH_{298}(H_3Si\text{–}H) = \Delta H°_{acid}(H_3Si\text{–}H) + EA(siH_3) - IP(H) \quad (10)$$

We find a $DH_{298}(H_3Si\text{–}H)$ = 90.3 ± 2.4 kcal/mol; this corresponds to a heat of formation of the silyl radical of $\Delta H_f°_{298}(SiH_3)$ = 46.4 ± 2.4 kcal/mol in excellent agreement with other determinations.[2] The heats of formation of Si, SiH, and SiH_2 could be established by ion chemistry through (10) if measured $\Delta H°_{acid}$ values for Si, SiH, and SiH_2 were available.[41] One way to tackle this is to study Si^-, SiH^-, and SiH_2^- charge exchange in a SIFT device; such studies are planned.

Very recently positive ion chemistry has been used in a very clear-cut way to establish the proton affinity of silylene.[51] A study of proton-transfer reactions of SiH_3^+ leads to a value of $\Delta H°_{acid}(H_3Si^+)$ = 201 ± 3 kcal/mol. Adoption of $\Delta H_f°_{298}(SiH_3^+)$ = 234.1 kcal/mol (from ref 15) and $\Delta H_f°_{298}(SiH_3)$ = 46.4 (from ref 2) then directly leads to a value of the heat of formation of silylene: $\Delta H_f°_{298}(SiH_2)$ = 69 ± 3 kcal/mol.

(46) The published expression[47] for Δ_{rot} is now known to be slightly incorrect. A derivation of (6) and a thorough analysis of this entire problem has been undertaken and will be published separately: Engelking, P. C. submitted for publication.

(47) Engelking, P. C.; Ellison, G. B.; Lineberger, W. C. *J. Chem. Phys.* **1978**, *69*, 1826.

(48) Engelking, P. C.; Lineberger, W. C. *J. Chem. Phys.* **1981**, *81*, 1234.

(49) Salomon, K. E.; Brauman, J. I. private communication.

(50) Hirota, E.; Kawaguchi, K. *Annu. Rev. Phys. Chem.* **1985**, *36*, 53. Yamada, C.; Hirota, E. *Phys. Rev. Lett.* **1986**, *56*, 923.

(51) Shin, S. K.; Beauchamp, J. L. *J. Phys. Chem.* **1986**, *90*, 1507.

VI. Conclusions

The experimental findings for SiH_3^+, SiH_3, and SiH_3^- are completely in accord with the qualitative ideas outlined in Figure 1. The SiH_3^- photodetachment spectra can be adequately modeled by using a single oscillator to describe the active mode in both the initial anion and the final silyl radical. The parameters for these umbrella potentials are found by choosing values which best fit the SiH_3^- spectrum (Figure 3). These potentials then accurately predict the SiD_3^- spectrum found in Figure 5. We have endeavored to "check" our potential for SiH_3 (derived from the SiH_3^- photoelectron spectra) by "predicting" the Franck-Condon profile of the SiH_3 photoionization spectrum: $SiH_3^+ \leftarrow SiH_3$. One's general ideas about valence (Figure 1) suggest that the umbrella potential for SiH_3^+ is a simple oscillator with a single minimum at $\xi_0 = 0°$; we appeal to the experiments outlined in ref 15 to establish that the umbrella oscillator for SiH_3^+ is a simple, linear oscillator with $\omega_2 = 820$ cm^{-1}. Our simulation of the SiH_3 photoionization spectrum is depicted in Figure 11 and fits the experimental findings.[15]

A summary of experimental properties is presented in Table V. The electron affinities, ionization potentials, vibrational frequencies (except for SiD_3^+), and heats of formation are all measured directly. Most of the molecular constants such as the inversion barrier, α(H-Si-H), and the rotational constants (B and C) are extracted from modeling experimental data. The accuracy of the silyl radical constants has recently been dramatically improved by the completion of an infrared diode laser absorption study.[50] This study reports the following values for SiH_3: α(H-Si-H) = 110.5°, r_0(Si-H) = 1.468 Å, and B ($v'' = 0$) = 4.763 15 cm^{-1}. The SiH_3 inversion barrier is estimated to be 1868 cm^{-1}. Our negative ion photoelectron results agree with these more precise values.

Acknowledgment. This paper is dedicated to Professor Peter P. Gaspar in honor of his award of the Frederic Stanley Kipping Award in Organosilicon Chemistry. We have had fruitful conversations with J. G. Radziszewski, J. Michl, and P. R. Bunker. We thank K. E. Salomon and J. I. Brauman for a preprint of their SiH_3^- photodetachment paper and for pertinent discussions. This work was supported by the U. S. Department of Energy (Contract No. DE-AC02-80ER10722). The VAX 11/750 digital computer used to carry out the Franck-Condon factor calculations was acquired with the help of the National Science Foundation CHE-8407084).

Registry No. SiH_4, 7803-62-5; SiH_3^-, 15807-96-2; SiD_3^-, 54637-68-2; SiH_3, 13765-44-1; SiD_3, 69103-84-0; NH_3, 7664-41-7.

Metal Cluster vs. Atom Reactivities. Calcium and Magnesium Vapor with Alkyl Halides and Methane

Kenneth J. Klabunde* and Alan Whetten

Contribution from the Department of Chemistry, Kansas State University, Manhattan, Kansas 66506. *Received April 4, 1986*

Abstract: Vapors of calcium and magnesium were codeposited with argon and argon/CH_3X mixtures (X = I, Br, Cl, F, H) at 9 K. Growth rates for Ca, Ca_2, Ca_x, Mg, Mg_2, Mg_3, Mg_4, and Mg_x in the presence and absence of CH_3X were monitored and reactivity trends established showing (a) clusters were more reactive than atoms, (b) larger clusters were more reactive than smaller clusters, (c) calcium species were more reactive than magnesium species, and (d) the reactivity trend for CH_3X was $CH_3I > CH_3F > CH_3Br > CH_3Cl$. Thermodynamic and ionization potential considerations seem to explain these trends.

We are interested in directly comparing chemical reactivities of ground-state atoms of the elements, and in comparing reactivities of small metal clusters with atoms. Recently we reported that Mg_2 and Mg_3 exhibited reactivity toward CH_3Br but Mg atoms did not.[1] Matrix isolation studies at low temperature sometimes allow such direct reactivity comparisons under exactly the same conditions of temperature, pressure, and concentration. Herein we report more complete studies on calcium and magnesium.

Background and Results

Calcium. The absorption spectra of calcium vapor species codeposited with inert gases have been studied in several laboratories.[2-4] Although there has been some disagreement over peak assignments, it is well-established that there is a strong atomic absorption due to the $4s4p \leftarrow 4s^2$ transition ($^1P_1 \leftarrow {}^1S_0$) near 410 nm (in argon). This transition appears as an asymmetric doublet corresponding to the 422.7-nm atomic transition in the gas phase. The splitting of this atomic band may be due to the non-O_h symmetry of the lattice causing a vacancy to be present next to the metal atom.[3] A sharp transition at 456 nm has been assigned as a forbidden $^1D_2 \leftarrow {}^1S_0$ atomic Ca transition.[2] It has been suggested that the symmetry of an incompletely substituted matrix site or a site containing a nearby impurity is reduced such that ^1P and ^1D have a common irreducible representation of approximately D_{3h} symmetry. Upon lowering the symmetry (from O_h), these two states can mix to give some observable intensity to the forbidden transition.[2]

Table I. UV-Visible Spectral Assignments for Matrix-Isolated Calcium Atoms, Dimers, and Clusters in Argon[a]

wavelength (nm)	species	assignment	ref
374	Ca_2	$^1\pi_u \leftarrow {}^1\Sigma_g^+$	5
415	Ca	$4s4p\ ^1P_1 \leftarrow 4s^2\ ^1S_0$	2,3
448[b]	Ca	$^1D_2 \leftarrow {}^1S_0$	2
470	Ca_x		
505	$Ca_x + Ca_2$		
550	Ca_x		
648	Ca_2	$^1\Sigma_u^+ (^1S + {}^1P) \leftarrow {}^1\Sigma_g^+ (^1S + {}^1S)$	7

[a] These are the bands observed in this work. Assignment are based on literature cited. [b] This band is questionable and we suspect it is not due to the atom. It was not considered for our reactivity comparisons.

(1) Imizu, Y.; Klabunde, K. J. *Inorg. Chem.* **1984**, *23*, 3602-3605.
(2) Andrews, L; Duley, W. W.; Brewer, L. *J. Mol. Spectrosc.* **1978**, *70*, 41-52.
(3) Francis, J. E., Jr.; Webber, S. E. *J. Chem. Phys.* **1972**, *56*, 5879-5886.
(4) Brewer, L.; Wang, J. L. F. *J. Chem. Phys.* **1972**, *56*, 4305-4309.

0002-7863/86/1508-6529$01.50/0